The VHF Doppler Radar as a Tool for Cloud and Precipitation Studies

KOICHIRO WAKASUGI* AND BEN B. BALSLEY

Aeronomy Laboratory, NOAA, Boulder, CO 80303

TERRY L. CLARK

National Center for Atmospheric Research,† Boulder, CO 80307

(Manuscript received 10 June 1986, in final form 8 October 1986)

ABSTRACT

The VHF Doppler radar has become a powerful tool for probing structures and motions of the clear air. In this paper, we discuss the capability of VHF radar as a tool for cloud and precipitation studies. Large fluctuations of refractive index from the cloudy air can be anticipated because of an abundance of water in clouds. Due to the difficulties in obtaining the necessary fine-scale observational data within clouds, we base our analysis of cloud-echoing properties on the numerical simulation of nonprecipitating cumulus by Klaassen and Clark. The Bragg scatter echo intensity is estimated from the temperature and humidity fields obtained from the cloud model. We find that the echo is enhanced at the boundary between the cloud and environment because of enhanced water vapor fluctuations. Although echoes from nonprecipitating clouds can be detected by UHF and VHF radars, only VHF radars can discriminate echoes due to large precipitation particles from the Bragg scatter echo of cloudy air. With UHF radars, the precipitation echoes totally mask the Bragg scatter echoes.

1. Introduction

Microwave Doppler radars have been very useful in studying the evolution of precipitating weather systems. The microwave radar echoes are derived mainly from cloud droplets and raindrops. Very high frequency (VHF) Doppler radars, on the other hand, are being used for probing the optically clear air. In this case, the radar pulse is scattered by refractive index fluctuations inherent in the turbulent air (e.g., Balsley and Gage, 1980).

Recently, VHF Doppler radar has been used to investigate tropospheric structures and motions during precipitating conditions (Larsen and Röttger, 1982; Fukao et al., 1985a; Wakasugi et al., 1985). Since VHF Doppler radars are capable of detecting echoes from both the refractive index fluctuation of air and precipitation particles, they are an ideal tool for accurately deriving raindrop size distribution (Fukao et al., 1985b; Wakasugi et al., 1986, 87). This is an important advantage in studies concerned with precipitation growth, cloud modeling, and microwave radio wave propagation.

In cloudy air, large fluctuations of atmospheric refractive index may be anticipated because there is an abundance of water in both liquid and vapor states in clouds. Radars operating at a 10 cm wavelength commonly observe nonprecipitating clouds (Gossard, 1979). Cloud observations have also been reported using a 7 m wavelength radar (Green et al., 1978).

In theory, the refractive index fluctuations in clouds arise from coupling between cloud dynamics and cloud microphysics. The process is difficult to understand, primarily because of the lack of accurate observational microphysical data. For example, Gossard (1979) has studied radar cloud echoes by using the results of a numerical cloud model because of the lack of observational data.

In this paper, we will discuss the concept of using the VHF Doppler radar as a tool for cloud and precipitation studies. Since the refractive index fluctuations within a cloud are a function of both temperature and humidity fields, the radar may be assumed to act as an overall sensor of these fields. After discussing the origins of radar echo from clouds following Gossard (1979), we estimate the refractive index fluctuation field of a nonprecipitating cloud based on a numerical cloud model. Our model involves results obtained by Klaassen and Clark (1985).

2. Radar echoes from clouds

As discussed by Gossard (1979), there are three possible mechanisms for radar backscattering from clouds: (1) classical Rayleigh scattering from randomly located liquid and/or ice particles; (2) Bragg scattering arising

* Permanent affiliation: Kyoto Institute of Technology, Matsugasaki, Kyoto 606, Japan.

† The National Center for Atmospheric Research is sponsored by the National Science Foundation.

from the spatial distribution of the particles; and (3) Bragg scattering from refractive index fluctuations in the gaseous medium due to atmospheric turbulence.

The first mechanism shows a classical inverse fourth-power wavelength dependence. The reflectivity factor Z is defined as

$$Z = \sum_{i=1}^{N} D_i^6 \tag{1}$$

where D_i is the diameter of particles. The summation is taken over all N-particles in a unit volume. Although the second and third mechanisms have been studied by Smith (1964) and Naito and Atlas (1966), the relative importance of these two mechanisms is still an open question. This is primarily because of the difficulties encountered in obtaining fine-scale observational data within clouds. However, Gossard (1979) has concluded theoretically that Bragg scatter from refractive index fluctuations in clouds due to gaseous water vapor is about 30 times more important than the Bragg scatter due to fluctuations in liquid water if the magnitude of variance of water vapor and liquid water are about equal. Therefore, in the following discussion we need to consider only mechanisms (1) and (3) as possible sources of radar backscatter from clouds.

In general, the radio refractive index n of air is a function of humidity, temperature and pressure (e.g., Kerr, 1951) such that

$$(n-1)\times 10^6 = (776P/T) + (6.00\times 10^3 Q_v P/T^2) \tag{2}$$

where pressure P is in kPa (100 kPa = 1000 mb), temperature T in K, and the moisture mixing ratio Q_v in g kg^{-1} (Q_v is the mass ratio of water vapor to dry air in the same volume). For discussion of the backscatter of radio waves, it is useful to consider the influence of the fluctuations in P, T and Q_v on n, rather than the absolute magnitude of n itself. The fluctuation of n can be expressed as

$$\delta n = \frac{\partial n}{\partial T}\delta T + \frac{\partial n}{\partial Q_v}\delta Q_v + \frac{\partial n}{\partial P}\delta P \tag{3}$$

where

$$\frac{\partial n}{\partial T} = -\frac{776P}{T^2} - 1.20\times 10^4 \frac{Q_v P}{T^3}$$

$$\frac{\partial n}{\partial Q_v} = 6.00\times 10^3 \frac{P}{T^2}$$

$$\frac{\partial n}{\partial P} = \frac{776}{T} + 6.00\times 10^3 \frac{Q_v}{T^2}$$

Thus, it would be possible to estimate δn if one could obtain data on T, Q_v, P and their fluctuation magnitudes at a specific point in the atmosphere. Moreover, because the δn fluctuations are statistically random in nature, it is necessary to discuss the variance of refractive index $\overline{\delta n^2}$ instead of δn itself. Although the overbar usually implies an ensemble average over different events, temporal or spatial average of observational data are used here for convenience.

In order to check the relative importance of fluctuations, we assume T = 280 K, P = 85 kPa and Q_v = 8 g kg^{-1}. This gives

$$\overline{\delta n^2}\times 10^{12} = 1.47\,\overline{\delta T^2} + 42.3\,\overline{\delta Q_v^2} - 15.8\,\overline{\delta T \delta Q_v} + O \tag{4}$$

where O denotes all of the terms in Eq. (3) related to pressure fluctuations. These terms can be safely neglected because the magnitude of δP seldom exceeds 1 Pa.

In the troposphere, although turbulent fluctuations in both T and Q_v are important, the δQ_v^2 term becomes a substantial part of $\overline{\delta n^2}$ even in "clear air" conditions. Indeed, Gossard (1977) discussed the refractive properties of tropospheric air masses, and concluded that the δQ_v^2 term is generally greater than that of δT^2 in the lower troposphere. Since the fluctuations of T and Q_v are dependent based on the Clausius–Clapyron equation (e.g., Pruppacher and Klett, 1978, p. 90), we need to check the possible role of the cross-product term $\overline{\delta T \delta Q_v}$ in Eq. (4) as pointed out by Gossard (1960).

It is very difficult to obtain observational data with sufficient resolution for estimating $\overline{\delta n^2}$ for Bragg scattering radar echo, since the spatial scales of interest (i.e., one-half the radar wavelength) are of the order of, or less than, 1 m. Even for the VHF band radar (e.g., λ = 6 m), the backscattered Bragg scale is $\lambda/2$ = 3 m, and the requisite spacing of data becomes 1.5 m if we take into account the result of the sampling theorem. The lack of observational data with this kind of resolution is mainly attributed to the slow response time of available sensors combined with the high speed of the aircraft carrying them. Furthermore, this kind of data is inadequate for estimating radar echoes because the data are usually collected only horizontally, while the radar is sensitive to fluctuations in other than horizontal directions. Therefore, in the following section, we will estimate $\overline{\delta n^2}$ in a cloud where the cloud parameters are based on microphysical data generated by a computer simulation.

3. The Klaassen–Clark small scale cumulus model

Klaassen and Clark (1985) have examined the mechanism of cloud entrainment by employing a numerical simulation of small nonprecipitating cumuli in the absence of shear. Grid nesting techniques permitted a very fine grid spacing of only 10 m in the vicinity of the entrainment regions. This resolution was obtained at the expense of restricting the simulation to two spatial dimensions.

The Klaassen–Clark model is very useful for estimating the $\overline{\delta n^2}$ field because it provides microphysical data such as water vapor content and temperature, as well as liquid water content and air motions within the

cloud. Although the 10 m grid spacing is still somewhat coarse from the radar backscatter point of view, it is far better than that available from conventional cloud simulations. It is reasonable to expect, therefore, that we can obtain an accurate estimate of δn^2 in clouds. Another interesting point of the model is that a negative correlation between δT and δQ_v might be anticipated when the ambient air outside the cloud is entrained into the cloud, and this could lead to the enhancement of δn^2 near the edge of the cloud.

The visible cloud shape is defined by the liquid water mixing ratio field Q_c (Q_c is the mass ratio of nonprecipitating liquid water to dry air in the same volume for the cloud model concerned). Figure 1 is an example of the Q_c field obtained at $t = 47.50$ min which is 14.50 min after the onset of moist convection. According to the Klaassen–Clark (1985) model, nodes appear on the upper cloud boundary, and a downdraft due to a cloud boundary baroclinic instability penetrates from the cloud top center into the interior of the cloud. This downdraft forms from the center-concave cloud top as shown in Fig. 1.

For our purposes, we need to define the fluctuation fields $\delta T(y, z)$ and $\delta Q_v(y, z)$ in addition to $T(y, z)$ and $Q_v(y, z)$ for deriving the total refractive index variance field $\delta n^2(y, z)$ from Eq. (3). Our definition for a fluctuation δX at a specific grid point (y_i, z_j) is given by $X(y_i, z_j) - \overline{X(y_i, z_j)}$ where $X = T$ or Q_v. The overbar in this case implies an average over a 5×5 grid point area whose center is at (y_i, z_j). For our 10 m spacing, this corresponds to a spatial average of 50×50 m^2 region. There are no substantial changes for the resultant fields when we choose a different number of grid points for averaging.

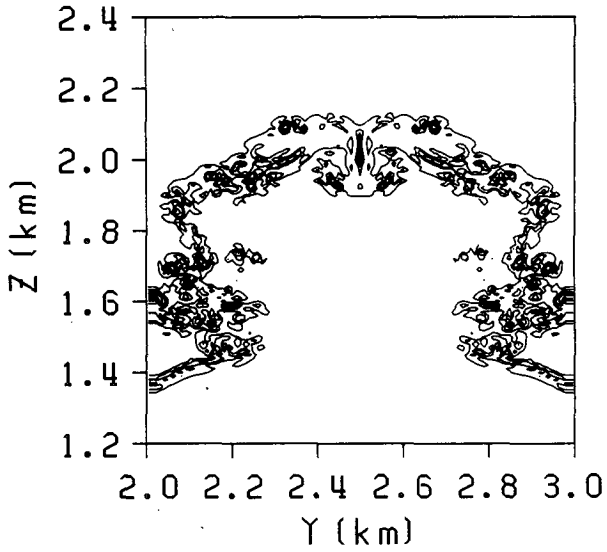

FIG. 2. The rms deviation of water vapor mixing ratio $\sqrt{\delta Q_v^2}$ corresponding to Fig. 1. The contour interval is 0.4 g kg^{-1} and the maximum rms value 2.4 g kg^{-1}.

Figures 2 and 3 show the root-mean-square (rms) values of δQ_v and δT fields corresponding to Fig. 1. The water vapor fluctuations shown in Fig. 2 are seen to occur just outside the cloud boundary defined by Q_c in Fig. 1. This is attributed to evaporation taking place at the interface between the cloud boundary and the environment. Figure 3, on the other hand, shows structure in the lower δT field due to the thermal circulation required to initiate cloud growth; this circulation was induced in the model by heating a limited surface region of the boundary layer.

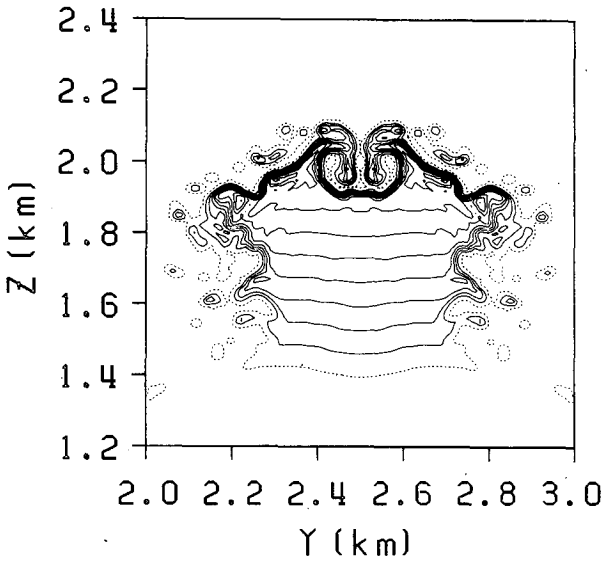

FIG. 1. Field plot of the liquid water mixing ratio Q_c for 47.50 min. The contour interval is 0.125 g kg^{-1} and the dotted line denotes the contour level of 0.01 g kg^{-1} (Klaassen–Clark cloud model.)

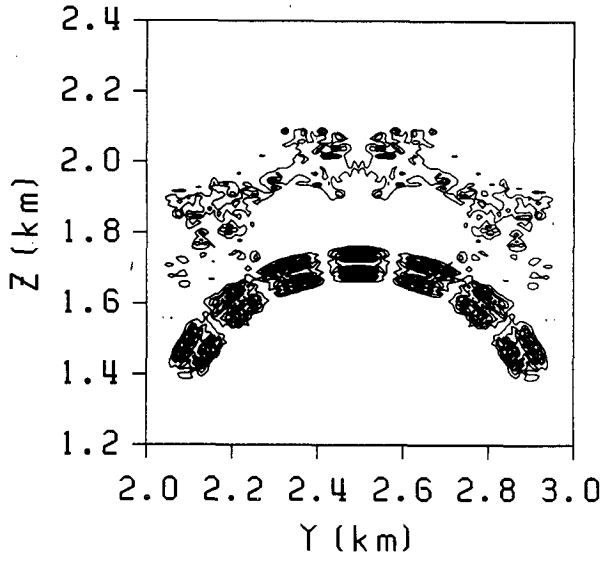

FIG. 3. The rms deviation of temperature $\sqrt{\delta T^2}$ corresponding to Fig. 1. The contour interval is 0.5 K and the maximum rms value 3.7 K.

It should be noted here that the maximum rms value of Q_c is 0.51 g kg^{-1}, while that of Q_v is 2.36 g kg^{-1}. Since the variance of Q_c is less than one-tenth of the Q_v variance, we can safely neglect the Bragg scatter component of echo as a result of the spatial distribution of cloud particles in the following discussions (Gossard, 1979).

Figure 4 shows the two-dimensional section of $\overline{\delta n^2}$ derived from Eq. (3). A remarkable enhancement of δn^2 can be seen at the interface of the environment and the cloud boundary as defined by the Q_c field in Fig. 1. Examination of Figs. 2 and 3 shows that the enhancement originates in the Q_v fluctuations rather than the temperature fluctuations. Moreover, the downdraft produces a noticeable structure in δn^2, penetrating downward from the cloud top at the center.

It is interesting to note that there have been two fundamental hypotheses for the entrainment mechanism in cumulus clouds. Stommel (1947) assumed that the ascending air parcel entrains air from its surroundings through the side of a cloud, while Squires (1958) proposed the importance of penetrative downdrafts from the cloud top. Squires' mechanism for cloud top entrainment relied upon mixing and the evaporative cooling of droplets. Even though the present results demonstrate one case of cloud top mixing, the mechanism driving the mixing appears to be quite different from that suggested by Squires. The present process is inviscid where it is driven by cloud boundary vorticity production and should be equally applicable to cloud side entrainment (see Klaassen and Clark (1985) for further discussion).

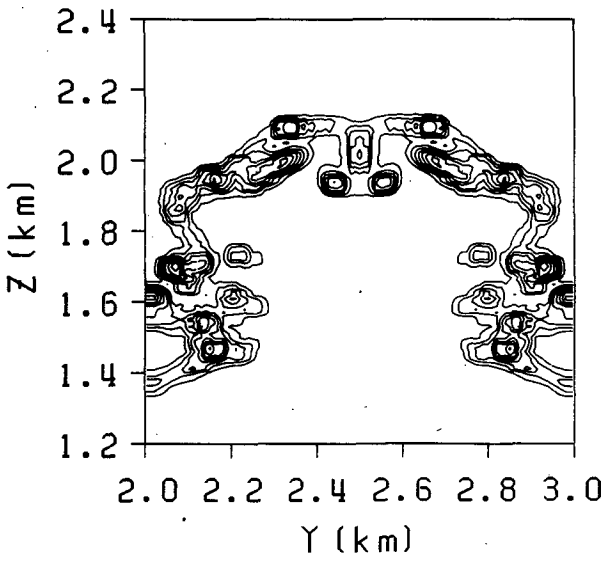

FIG. 4. Field plot of the refractive index variance $\overline{\delta n^2}$ at the time of 47.50 min. The contours are in a linear scale and the interval is 10. The minimum level corresponds to $\overline{\delta n^2} = 1.0 \times 10^{-12}$ and the maximum value is 9.0×10^{-11}.

Figure 5 shows the evolution of $\overline{\delta n^2}$ structure with time beginning much earlier than portrayed in Figs. 1–3, and extending to much later periods in the cloud evolution. In the early period of the cloud evolution, $\overline{\delta n^2}$ is mainly due to the δT^2 term because the Q_v field is still stably laminated and has not been perturbed from the initial environmental condition (see Fig. 3). The δQ_v^2 contribution becomes dominant and grows with time. At the final stage of evolution, the $\overline{\delta n^2}$ field shows a depression of the cloud top resulting from the downdraft penetration into the cloud.

A domelike structure of radar returns in clear air conditions has been reported in many cases by Atlas (1959), Hardy and Ottersten (1969), Gossard et al. (1971), among others. Gossard (1960) pointed out the importance of negative correlation in $\delta T \delta Q_v$ as an origin of these radar returns. This effect clearly arises as a result of the entrainment of dry air into the moist rising air at the boundary of the thermal or plume type updraft.

In Fig. 6, we present the correlation field $\overline{\delta T \delta Q_v}$ at the time corresponding to Fig. 4. The correlation is essentially positive inside the cloud due to adiabatic rising of saturated air, while a negative correlation exists outside the cloud because of evaporation of cloud liquid water. However, this negative correlation does not enhance the cloud refractive index variance δn^2 as much as is the case in clear air conditions. This is because the fluctuation in water vapor δQ_v^2 dominates δn^2 in "cloudy air" conditions. Indeed, the maximum value of δn^2 decreases only by 20% when we neglect the $\delta T \delta Q_v$ term in the example of Fig. 4.

The Klaassen–Clark model produces wind fields as well as Q_c, Q_v, and T fields. This makes it possible to derive a Doppler histogram corresponding to an estimate of Doppler spectrum of radar echo. Here we compute the Doppler histogram in terms of the line-of-sight velocity histogram of grid points weighted by the magnitude of δn^2 at each grid point in a finite radar volume. We have neglected the effects such as the curvature of radar pulse wavefront and receiver noise in our computations. Figure 7 shows an example of echo intensity contour in Doppler velocity and height (the velocity interval is 0.1 m s^{-1}). We proceed to observe the cloud by using a vertically pointing antenna beam at $y = 2.5$ km, i.e., at the center of the cloud. In this case the beam width is fixed to be 100 m at any height (a typical value for VHF Dopplar radar). The height resolution is 10 m which is kept equal to the grid spacing.

Figure 4 shows a downdraft reaching -4 m s^{-1} near the cloud top; this produces the entrainment of air, resulting in the concave shape of the $\overline{\delta n^2}$ field at the cloud top as indicated in Fig. 4. The estimated spectral width (i.e., the half-power width of the principal peak) is $\sim$0.1 m s^{-1} in the figure. This is narrower than the typical values ($\sim$0.5 m s^{-1}) expected from typical radar observations. This is partly due to a 10 m height res-

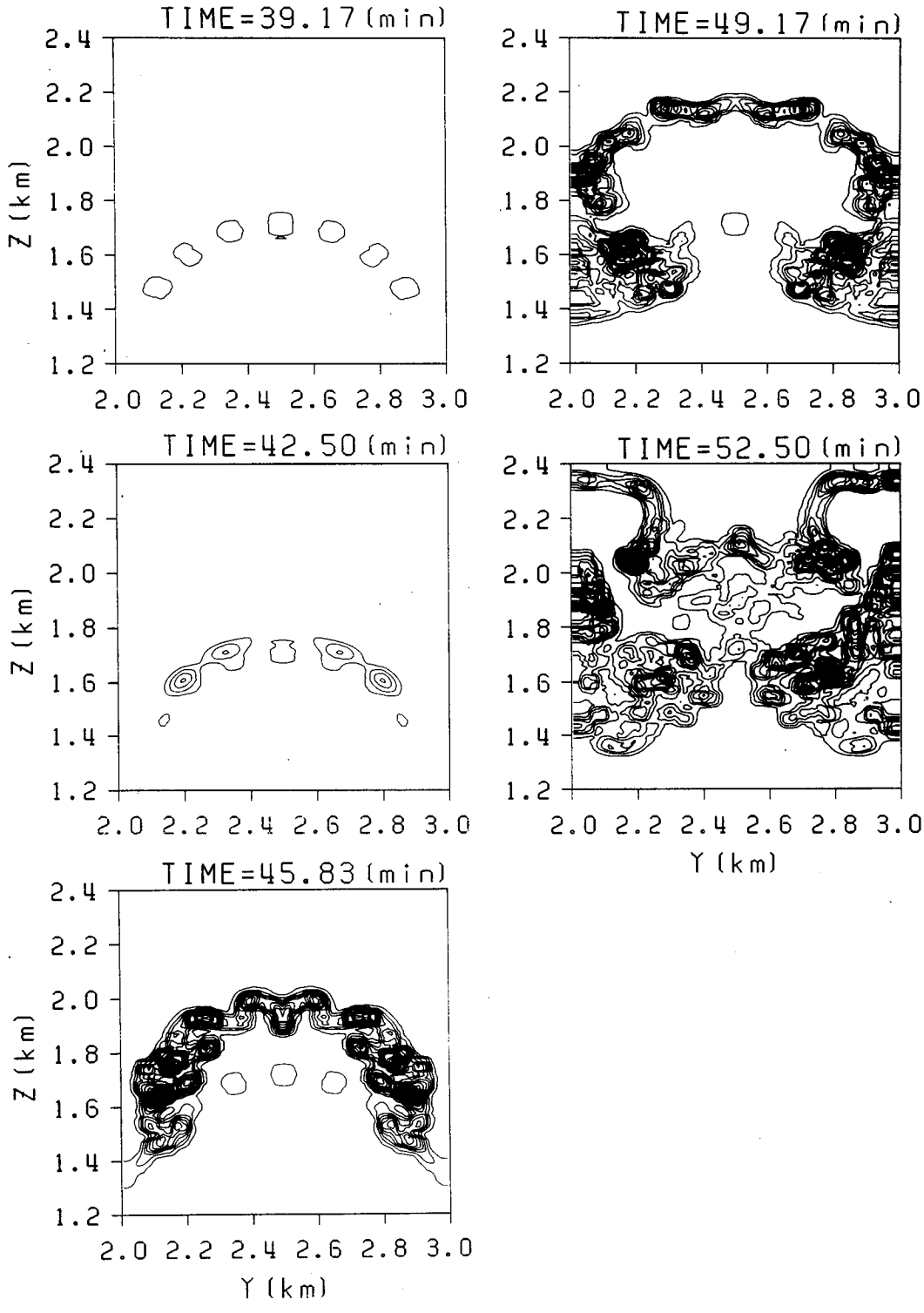

FIG. 5. Time evolution of the refractive index variance field $\overline{\delta n^2}$ from 39.17 to 52.50 min. The contours are in a linear scale and the minimum level corresponds to $\overline{\delta n^2} = 1.0 \times 10^{-12}$.

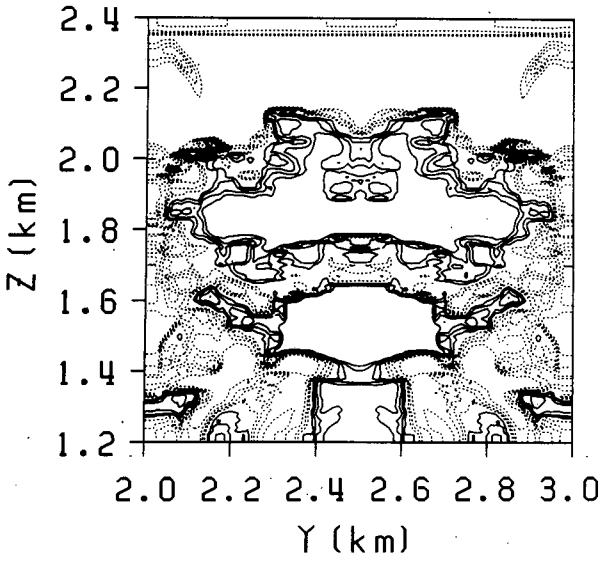

FIG. 6. Correlation field of $\overline{\delta T \delta Q_v}$ at 47.50 min. The correlation is defined by $\overline{\delta T \delta Q_v}/\sqrt{\delta T^2 \delta Q_v^2}$. The contour level is 0.2 and the negative correlation is plotted by dotted curves.

olution of this example compared to a more typical radar resolution of $\geq$100 m. Furthermore, the subgrid motions, which are parameterized by the Lilly (1962) and Smagorinski (1963) type stress tensor in the model, result in the exclusion of scales smaller than 10 m. Recall that our grid spacing is coarse compared to the Bragg wavelength ($\lambda/2$) for radar backscatter, although the grid spacing of the model is far better than that of a conventional cloud model.

4. Discussion and conclusions

We have discussed the usefulness of the clear-air Doppler radar as a tool for cloud studies. Our estimates of Bragg scatter from the refractive index fluctuations of nonprecipitating clouds is based on the numerical cloud model of Klaassen and Clark (1985). Our results show that enhanced radar echoes are expected at the boundary between the cloud and the environment. These enhancements arise primarily because of the humidity fluctuations (as opposed to thermal fluctuations). The echo enhancement due to the negative correlation of $\delta T \delta Q_v$ is less important with a cloud relative to the clear air case.

Although the numerical model we have used is one of the finest spacial resolutions currently available, the spacing is too coarse for the requisite wavelength for Bragg scatter radar echo. This problem worsens for numerical models of precipitating clouds because such models need more state variables of water. This leads to computer memory restrictions with a resulting poorer spatial resolution of the cloud model. However, observational results show the enhanced echoes have also been detected for precipitating clouds.

Figure 8 is an example of VHF Doppler spectra obtained during a precipitation event (Wakasugi et al., 1986). Below the (~5 km) melting level, the two peaks of the bimodal spectra correspond to the echoes from air and precipitation particles. Those peaks are spectrally separated because of the particle motion relative to the ambient air. Typical values are $C_n^2 = 10^{-14}$ to 10^{-16} and $Z = 10^2$ to 10^4 below the melting level. The echo intensities are, roughly speaking, of the same order for VHF radar observations. (At shorter wavelength, precipitation echoes totally mask echoes from Bragg scatter of refractive index fluctuations due to the inverse fourth-power wavelength dependence.) However, echoes that are both enhanced in intensity and broadened in spectral width are occasionally observed as indicated by the spectra at 0830 LST above the melting level. (The spectra at 0752 and 0909 LST are more typical ones.) The enhanced echoes are usually observed accompanying a strong updraft, indicating an importance of air mass mixing of different kinds. Further work is needed based on radar observations as well as numerical cloud models.

It can be possible to probe cloudy air by existing mesosphere–stratosphere–troposphere (MST) type radars. However, there is a difficulty in measuring the lower tropospheric region by the existing MST radars. This is due to receiver dynamic range problems as well as problems involving the transmitter/receiver (T/R) switch recovery of the system. Typically, these radars were originally designed for atmospheric studies at heights $\geq$ 3–4 km. For studies at lower heights, (e.g., for cloudy air probing) it is possible to design a so-called boundary layer radar which could begin mea-

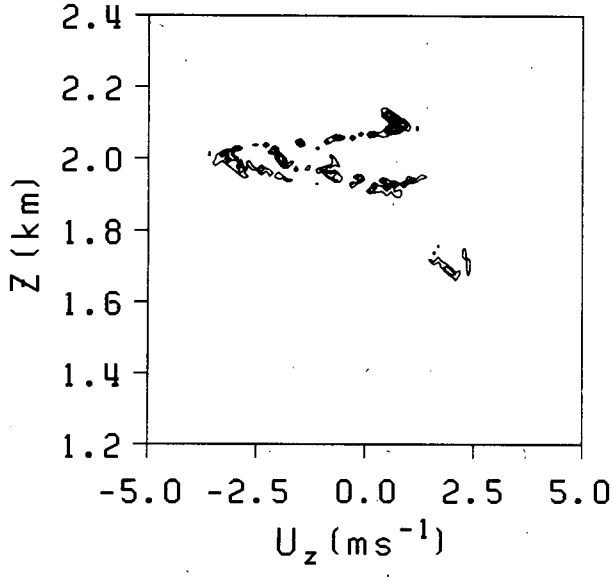

FIG. 7. Doppler echo intensity contour at the time of 47.50 min. Vertically pointing antenna at y = 2.5 km is assumed. The beam width and height resolution are fixed at 100 m and 10 m, respectively.

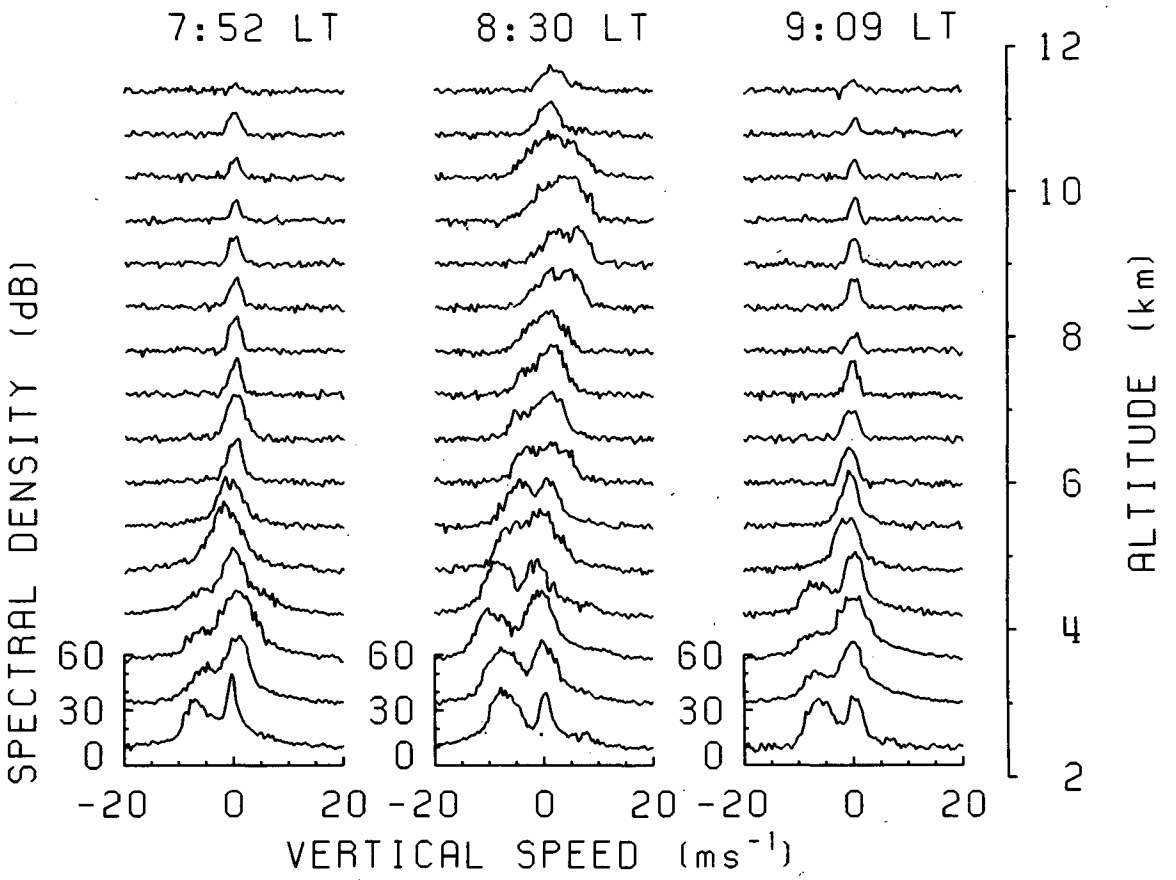

FIG. 8. An example of VHF Doppler spectra observed with vertically pointing beam. Spectra at 0752 and 0909 LST are normal ones, while spectra at 0830 LST above the melting level (~5 km) are enhanced in intensity and broadened in width. Below the melting level, the spectral peaks with a relatively small vertical speed correspond to the echo from refractive index fluctuations of air. The other peaks with a large negative speed originate from the precipitation particles (Wakasugi et al., 1987).

surements at a few hundred meters and which would be capable of much finer height resolution (Balsley and Ecklund, personal communications, 1986). We suggest here an alternative approach, which involves installing a small receive-only antenna nearby the existing system. (We assume that the system under consideration has a sufficient good height resolution.) Since a relatively strong echo is anticipated from the lower troposphere, it would be possible to operate the small receiving antenna and the existing ("transmitting") antenna as a bistatic radar system. This would minimize T/R switching problems, and the existing receiver and signal processing systems could be used without additional costs for probing cloudy air almost to ground level.

Acknowledgments. This work was done while one of us (KW) was staying at the Aeronomy Laboratory/NOAA as a Guest Researcher supported by the Ministry of Education, Culture and Science, Japan. We thank Earl E. Gossard for constructive suggestions and Helen Axtell for typing the manuscript.

REFERENCES

Atlas, D., 1959: Meteorological angel echoes. *J. Meteor.*, **16,** 6–11.

Balsley, B. B., and K. S. Gage, 1980: The MST radar technique: Potential for middle atmospheric studies. *Pure Appl. Geophys.*, **119,** 452–493.

Fukao, S., K. Wakasugi, T. Sato, T. Tsuda, I. Kimura, N. Takeuchi, M. Matsuo and S. Kato, 1985a; Simultaneous observation of precipitating atmosphere by VHF band and C/Ku band radars. *Radio Sci.*, **20,** 622–630.

——, ——, ——, S. Morimoto, T. Tsuda, I. Hirota, I. Kimura and S. Kato, 1985b: Direct measurement of air and precipitation particle motion by VHF Doppler radar. *Nature,* **316,** 712–714.

Gossard, E. E., 1960: Power spectra of temperature, humidity and refractive index from aircraft and tethered balloon measurements. *IEEE Trans. Antennas. Propag.*, **AP-8,** 186–201.

——, D. R. Jensen and J. H. Richter, 1971: Analytical study of tropospheric structure as seen by high-resolution radar. *J. Atmos. Sci.*, **28,** 794–807.

——, 1977: Refractive index variance and its height distribution in different air masses. *Radio Sci.*, **12,** 89–105.

——, 1979: A fresh look at the radar reflectivity of clouds. *Radio Sci.*, **14,** 1089–1097.

——, and R. G. Strauch, 1983: *Radar Observation of Clear Air and Clouds,* Elsevier, Amsterdam, 280 pp.

Green, J. L., R. H. Winkler, J. M. Warnock, W. L. Clark, K. S. Gage

and T. E. VanZandt, 1978: Observations of enhanced clear air reflectivity associated with convective clouds, *18th Conference on Radar Meteorology,* Amer. Meteor. Soc., Atlanta, GA, 88–93.

Hardy, K. R., and H. Ottersten, 1969: Radar investigations of convective patterns in the clear atmosphere. *J. Atmos. Sci.,* **26,** 666–672.

Kerr, D. E., 1951: *Propagation of Short Radio Waves,* Dover, 728 pp.

Klaassen, G. P., and T. L. Clark, 1985; Dynamics of the cloud-environment interface and entrainment in small cumuli: Two-dimensional simulations in the absence of ambient shear. *J. Atmos. Sci.,* **42,** 2621–2642.

Larsen, M. F., and J. Röttger, 1982: VHF and UHF Doppler radars as tools for synotpic research. *Bull. Amer. Meteor. Soc.,* **63,** 996–1008.

Lilly, D. K., 1962: On the numerical simulation of buoyant convection. *Tellus,* **14,** 148–172.

Naito, K., and D. Atlas, 1966: On microwave scatter by partially coherent clouds. *12th Weather Radar Conf.,* Amer. Meteor. Soc., Boston, MA, 7–12.

Pruppacher, H. R., and J. D. Klett, 1978: *Microphysics of Clouds and Precipitation,* Reidel, Holland, 714 pp.

Smagorinski, J., 1963: General circulation experiments with the primitive equations. I: The basic experiment. *Mon. Wea. Rev.,* **91,** 99–164.

Smith, R. L., 1964: Scattering of microwaves by cloud droplets, *11th Weather Radar Conference,* Amer. Meteor. Soc., Boulder, CO, 202–207.

Squires, P., 1958: Penetrative downdraughts in cumuli. *Tellus,* **10,** 381–389.

Stommel, H., 1947: Entrainment of air into a cumulus cloud. *J. Meteor.,* **4,** 91–94.

Wakasugi, K., S. Fukao, S. Kato, A. Mizutani and M. Matsuo, 1985: Air and precipitation particle motions within a cold front measured by the MU VHF radar. *Radio Sci.,* **20,** 1233–1240.

——, A. Mizutani, M. Matsuo, S. Fukao and S. Kato, 1986: A direct method for deriving drop-size distribution and vertical air velocities from VHF Doppler radar spectra. *J. Atmos. Oceanic Technol.,* **3,** 623–629.

——, ——, ——, —— and ——, 1987b: Further discussion for deriving dro-size distributions and vertical air velocities directly from VHF Doppler radar spectra. *J. Atmos. Oceanic Technol.,* **4,** 170–179.